


## RESEARCH ARTICLE

# Continuous modelling of single layer 2D carbon nanostructures based on a modified Cauchy–Born rule

Julian Ochs  | Jens Wackerfuß

Institute of Structural Analysis, University of Kassel, Kassel, Germany

## Correspondence

Julian Ochs, Institute of Structural Analysis, University of Kassel, Kassel, Germany.  
Email: [Ochs@uni-kassel.de](mailto:Ochs@uni-kassel.de)

## Abstract

Graphene is the thinnest known structure. It consists of a single layer of carbon atoms and has unique mechanical properties. The carbon atoms form bonds with neighbouring atoms that can be described by interatomic potentials. A simulation of molecular mechanical processes can be performed by applying the formalism of the finite element method to the interatomic potentials. Neglecting local effects, a continuum formulation is an efficient alternative to a discrete model. The continuum formulation requires a connection between the discrete atomic lattice and the continuum. One way of doing this is to use the CAUCHY–BORN rule. This paper reviews the extensions of the CAUCHY–BORN rule, in particular, the exponential CAUCHY–BORN rule, and adds an alternative approach. It is shown that all contributions dealing with the exponential Cauchy–Born rule inevitably lead to shell models with KIRCHHOFF–LOVE kinematics. The approach presented here instead uses a shell model with REISSNER–MINDLIN kinematics, which has the major advantage of a much simpler mesh generation and a simpler application of the boundary condition.

## KEYWORDS

Cauchy–Born hypothesis, extension Cauchy–Born hypothesis, graphene-based nanostructures, homogenisation, Reissner–Mindlin shell element

## 1 | INTRODUCTION

Graphene is the thinnest membrane structure known [1]. It consists of a single layer of carbon atoms and has unique mechanical, electrical and chemical properties. Graphene has a wide range of applications, for example, electronic devices such as transistors [2, 3] and solar cells [4]. The internal energy of graphene can be described in terms of interatomic potentials ( $E_{\text{atom}}$ ). These potentials measure the interaction between the atoms. They depend on the atomic kinematics (see Figure 1).

$$E_{\text{atom}} = E_{\text{atom}}(r, \theta, \varphi, \psi, \chi) \quad (1)$$

The standard way to simulate these discrete systems is the molecular dynamics [5], but it is also possible to embed the simulations in the formalism of the finite element method [6, 7]. If we assume that local effects such as the breaking of

This is an open access article under the terms of the [Creative Commons Attribution-NonCommercial](https://creativecommons.org/licenses/by-nc/4.0/) License, which permits use, distribution and reproduction in any medium, provided the original work is properly cited and is not used for commercial purposes.

© 2023 The Authors. *Proceedings in Applied Mathematics and Mechanics* published by Wiley-VCH GmbH.

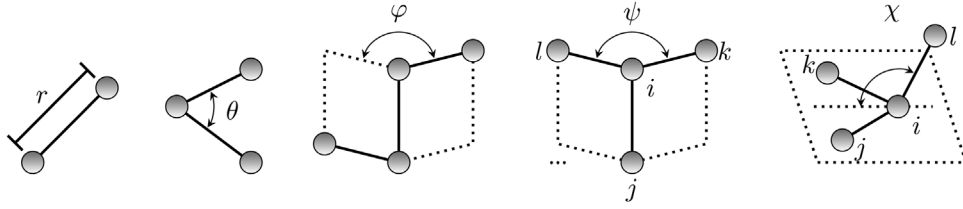


**FIGURE 1** Atomic kinematics: bond length  $r$ , valence angle  $\theta$ , dihedral angle  $\varphi$ , improper dihedral angle  $\psi$ , inversion angle  $\chi$ .

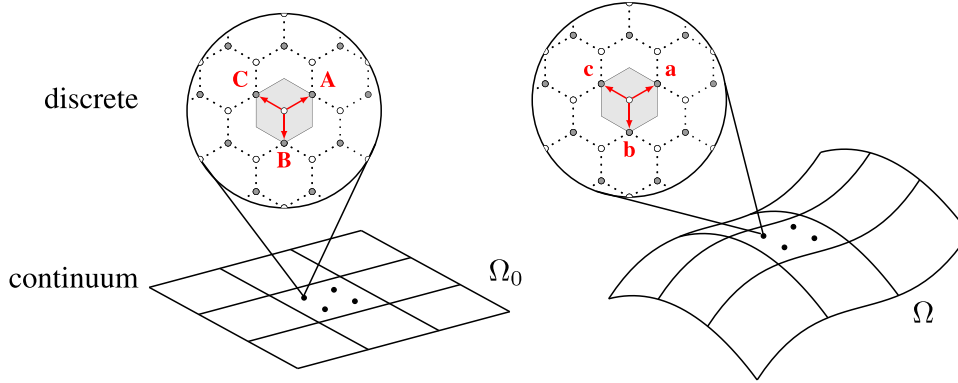


**FIGURE 2** Multiscale approach: discrete and continuous region (reference  $\Omega_0$  and current configuration  $\Omega$ ).

existing bonds or the formation of new bonds do not occur, we can say that the discrete simulations are inefficient. A more promising approach is to formulate a continuum theory based on interatomic potentials and derive the finite element approximation. The idea is, therefore, to develop a constitutive equation for a shell element that has the mechanical properties of graphene. To achieve this, the internal energy of graphene is homogenised to obtain the strain-energy density. The material model is then derived from the strain-energy density. To incorporate the strain-energy density into the shell formulation, the discrete region of the atomic lattice (see Figure 2) and the continuous region of the shell must be linked. This linkage can be done with the CAUCHY–BORN rule.

## 2 | THE STANDARD CAUCHY–BORN RULE AND EXTENSIONS

The Cauchy–Born rule is a kinematic assumption and the standard approach for incorporating atomistic potentials into continuum theory [8, 9]. The CAUCHY–BORN rule states that the infinitesimal material tangents in classical continuum mechanics deform in the same way as the lattice vectors of a space-filling crystals (see Figure 3). According to this, a lattice vector with the deformation gradient can be transformed from the reference configuration to the current configuration in the following way.

$$\mathbf{a} = \mathbf{F}\mathbf{A} \quad (2)$$

This assumption is valid for space-filling crystals (Figure 3). For curved surfaces or shell-like structures, the assumption is not valid. This is because the deformation gradient only transforms a vector  $\mathbf{A}$  from one tangential space  $\mathcal{T}_{\mathbf{x}}\Omega_0$  into the other  $\mathcal{T}_{\mathbf{x}}\Omega$ . For a correct evaluation of the interatomic potentials, it needs the vector  $\mathbf{a}$  (see Figure 4) on the surface. The classical CAUCHY–BORN rule, therefore, requires an extension, which makes it possible to map from the tangential space to the surface. In classical continuum mechanics (BOLTZMANN continuum), the material information is usually only needed at one point. However, this approach also requires non-local information about the surrounding surface at that point. This gives the problem a non-local character. There are two main concepts of extension in the literature. The higher-order CAUCHY–BORN rule [10] and the exponential CAUCHY–BORN rule [11–13]. The higher-order CAUCHY–BORN rule performs a Taylor expansion of the deformation gradient and stops after the second term. The resulting quadratic component in the deformation gradient can be interpreted as a correction factor that ‘pulls’ the vector back to the surface. The

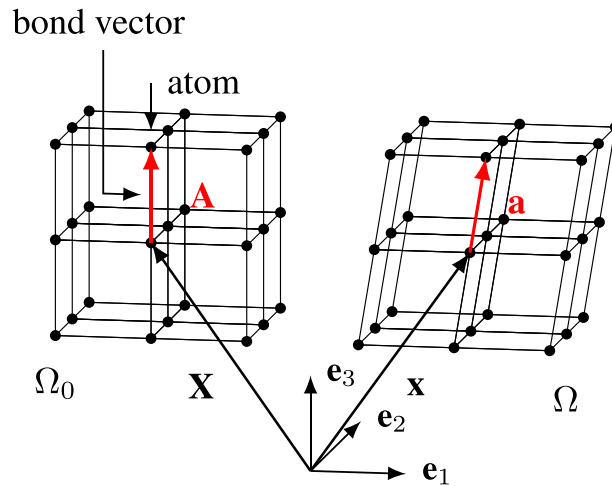


**FIGURE 3** CAUCHY-BORN rule for space filling crystals: The lattice vectors are transformed correctly.

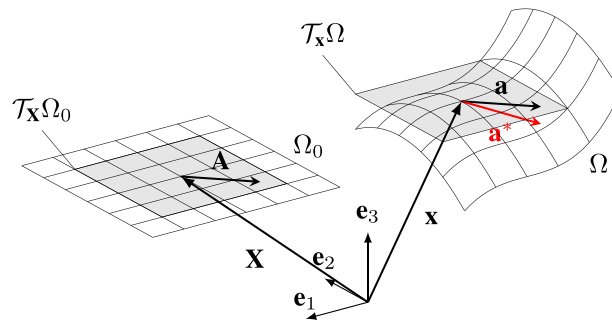


**FIGURE 4** CAUCHY-BORN rule for shell-like structures: The lattice vectors are only transformed in the tangent space.

exponential CAUCHY-BORN rule uses an ‘exponential map’ to map from the tangent space to the surface. The following discussion only deals with the exponential CAUCHY-BORN rule. Therefore, a brief overview of exponential mapping procedures is given below.

## 2.1 | Exponential mapping on two cylinders

ARROYO and BELYTSCHKO [11] use an exponential map to extend the CAUCHY-BORN rule. An exponential map uses the geodesics of the surface to map from the tangent space onto the surface. For arbitrarily shaped surfaces, the geodesics can not be calculated analytically and must be calculated numerically. To avoid the high computational cost of the additional numerical problem, the exponential map is approximated in this approach. The exponential map is approximated by an exponential map on two cylinders, for which the geodesics can be calculated analytically. The cylinders are constructed from an eigenvalue problem involving the metric of the surface  $\mathbf{C}$  and the curvature tensor  $\mathbf{K}$ . The eigenvalues correspond to the maximum or minimum curvature and the eigenvectors specify the corresponding directions. A cylinder is now constructed for each direction. The radius corresponds to the reciprocal eigenvalue. With the two cylinders, it is possible to formulate two correction terms that pull the vector onto the surface. The mapping procedure is then as follows: Starting from a planar reference configuration, first the vector in the reference configuration  $\mathbf{A}$  with the deformation gradient is mapped into the tangential space of the current configuration  $\mathbf{a}$ . Then the vector is mapped from the tangential space of the current configuration onto the surface  $\mathbf{a}^*$  with the exponential map (Figure 5). The original approach is limited to planar reference configurations. Through the extension of FINDEISEN and WACKERFUß [12], it is also possible to consider arbitrarily shaped reference configurations. For this purpose, an inverse exponential mapping is formulated. This maps the vector from the surface of the reference configuration  $\mathbf{A}^*$  into the tangential space of the reference configuration  $\mathbf{A}$ . The complete mapping procedure from the surface in the reference configuration to the surface of the current configuration

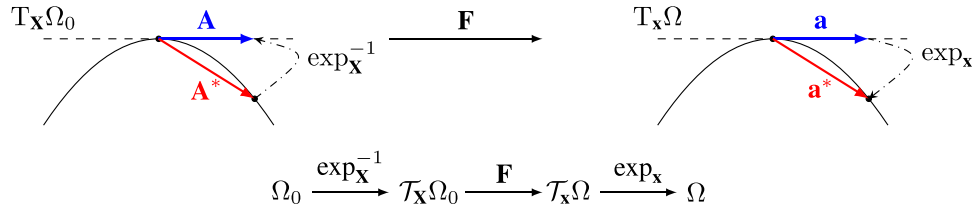


**FIGURE 5** Mapping procedure from the surface of the reference config. to the surface of the current config.

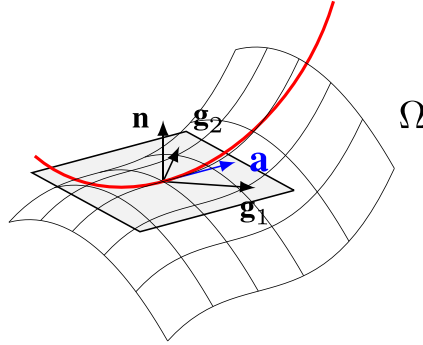


**FIGURE 6** Tangent space of the current configuration with the construction of the circle (red).

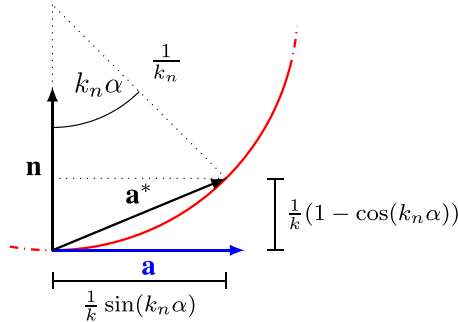


**FIGURE 7** Mapping on the circle;  $\alpha = \|\mathbf{a}\|$ .

can be seen in Figure 5. The advantage of the inverse exponential mapping is that it allows curved surfaces to be considered. Without this improvement, pre-processing always had to be done by first ‘rolling up’ the planar reference configuration. This limits the range of significant geometries to those that can be rolled up, such as cylinders. Complicated geometries such as junctions of cylinders cannot be modelled without the extension.

## 2.2 | Exponential mapping on circle

HOLLERER and CELIGOJ [13] also used an exponential map to map the vector from the tangent space to the surface. Here the exponential map is approximated by mapping onto a single circle. The circle is constructed in the direction the considered vector is pointing at (Figure 6). The radius of the circle is the reciprocal of the local curvature. The local curvature  $k_n$  is calculated by projecting the curvature tensor  $\mathbf{K}$  onto the normalised vector in tangent space (see Equation 6 left side). The mapping onto the circle can then be represented with the sine and cosine functions (Figure 7). This approach is restricted to planar reference configurations. It has the same pre-processing difficulties as in Arroyo and Belytschko [11]. The advantage of this approach is that no eigenvalue problem needs to be solved. The new approach should be based on this approach.

**TABLE 1** Comparison of the approaches presented.

	[11]	[12]	[13]	New approach
Eigenproblem	Y	Y	N	N
Arbitrary ref. config.	N	Y	N	N <sup>a</sup>
Analytical stiffness	N	N	Y	Y
Separation mat./FE	N	N	Y	Y
Strains	<b>C, K</b>	<b>C, K</b>	<b>c, k</b>	<b>ε, κ, γ</b>
Shell model	K-L	K-L	K-L	R-M
FE formulation	Special	Special	Special	Standard
DOFs	<b>u</b>	<b>u</b>	<b>u</b>	<b>u, φ</b>

Abbreviations: K-L, KIRCHHOFF–LOVE; R-M, REISSNER–MINDLIN

<sup>a</sup>Currently.

### 3 | NEW APPROACH

The approaches presented construct the mapping procedure using the metric tensor **C** and the curvature tensor **K**. In all the publications mentioned, this leads inevitably to a shell model with KIRCHHOFF–LOVE kinematics. All authors used subdivision elements [14] to treat the KIRCHHOFF–LOVE theory. These elements have several disadvantages. The first is that the mesh generation and the boundary condition application is not as easy as for standard finite elements, and the second is that the element formulation only involves translational degrees of freedom. The approach presented here is based on a shell with REISSNER–MINDLIN kinematics and a standard finite element formulation. The main advantage is that the two disadvantages of the sub-division elements do not occur here. Table 1 shows a detailed comparison of the approaches discussed. In the following, a constitutive equation for a REISSNER–MINDLIN shell is derived. This involves deriving the stress resultants vector and the tangential material matrix. The starting point is the strain-energy density function of the atomic lattice. The strain-energy density function is obtained by considering the interatomic potentials in a representative cell. In order to evaluate these, the position of the atomic lattice on the surface of the current configuration must first be known. The position of the atomic lattice is computed here using the Cauchy–Born rule and extensions. Like HOLLERER’s approach [13], this approach allows a complete separation of the constitutive relation and the finite element formulation. This makes it possible to use a standard ‘user material’ interface of an existing FE code. The input to this ‘user material’ are the strains and the output is the stress resultants vector and the material matrix. The details of the calculation are discussed in the next sections. The advantage of this approach is that a standard shell element can be used and graphene-based nanostructures can be calculated using this material box. Furthermore, all existing improvements for the REISSNER–MINDLIN shell, for example, to avoid locking effects, can be used.

#### 3.1 | Mapping procedure with the new approach

Several extensions to the standard CAUCHY–BORN rule were presented. The mapping procedures were based on the KIRCHHOFF–LOVE kinematics. Here, an approach based on the REISSNER–MINDLIN strains is derived.

$$\boldsymbol{\varepsilon} = \varepsilon_{\alpha\beta} \mathbf{G}^\alpha \otimes \mathbf{G}^\beta; \quad \boldsymbol{\kappa} = \kappa_{\alpha\beta} \mathbf{G}^\alpha \otimes \mathbf{G}^\beta; \quad \boldsymbol{\gamma} = \gamma_\alpha \mathbf{G}^\alpha \quad (3)$$

$$\varepsilon_{\alpha\beta} = \frac{1}{2}(\mathbf{g}_\alpha \cdot \mathbf{g}_\beta - \mathbf{G}_\alpha \cdot \mathbf{G}_\beta); \quad \kappa_{\alpha\beta} = \frac{1}{2}(\mathbf{g}_\alpha \cdot \mathbf{d}_\beta + \mathbf{g}_\beta \cdot \mathbf{d}_\alpha) - \frac{1}{2}(\mathbf{G}_\alpha \cdot \mathbf{D}_\beta + \mathbf{G}_\beta \cdot \mathbf{D}_\alpha); \quad \gamma_\alpha = \mathbf{g}_\alpha \cdot \mathbf{d} - \mathbf{G}_\alpha \cdot \mathbf{D} \quad (4)$$

When deriving the stress tensor and the tangential material tensor, a case distinction must be made. In general, the extension of the CAUCHY–BORN only makes sense if the loading is not purely in-plane. In other words: If the shell moves only in the tangential space, the extension is not required.

##### 3.1.1 | Case: Pure membrane load – standard CAUCHY–BORN rule

For a pure membrane load, the standard CAUCHY–BORN is sufficient. The only step is to apply the CAUCHY–BORN rule (2).

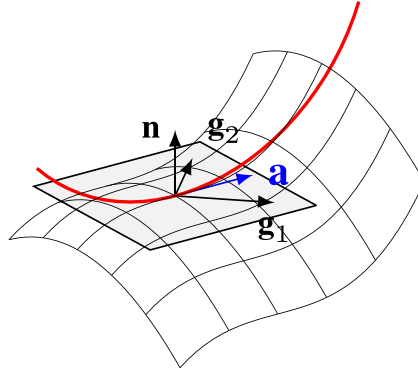


**FIGURE 8** Tangent space of the current configuration with the construction of the osculating circle.

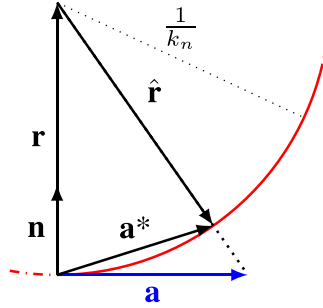


**FIGURE 9** Mapping onto the circle.

### 3.1.2 | Case: Non-pure membrane load – extension of the CAUCHY–BORN rule

This approach is based on HOLLERERS [13] approach. The first step is to apply the standard CAUCHY–BORN rule (2). This transforms the bond vectors from the tangent space of the reference configuration  $\mathbf{A}$  to the tangent space of the current configuration  $\mathbf{a}$ . The next step is to map the vector from the tangent space onto the surface. This is done using a ‘radial return’ approach. Unlike the previous approaches, this one does not require the geodesics of the surface to be computed. No trigonometric functions are used. The mapping procedure starts by constructing a circle with the inverse of the local curvature (Figure 8). Then we construct two vectors. The first vector runs from the end of vector  $\mathbf{a}$  to the centre of the circle and the second vector runs from the centre of the circle to the edge of the circle in the direction of the tip of  $\mathbf{a}$  (Figure 9). The mapping can then be written as the addition of the vectors  $\mathbf{r}$  and  $\hat{\mathbf{r}}$ .

$$\mathbf{a}^* := \hat{\mathbf{r}} + \mathbf{r}; \quad \mathbf{r} := \frac{1}{k_n} \mathbf{n}; \quad \hat{\mathbf{r}} := \frac{1}{k_n} \frac{\mathbf{a} - \mathbf{r}}{\|\mathbf{a} - \mathbf{r}\|} \quad (5)$$

The local curvature  $K_n$  can be calculated by projecting the bending strains onto the normalised vector  $\mathbf{a}$ . The following expression results for the current and the reference configuration ( $\boldsymbol{\kappa}^c$  are the bending strains defined in the current configuration):

$$k_n = \frac{\mathbf{a}}{\|\mathbf{a}\|} \cdot \boldsymbol{\kappa}^c \cdot \frac{\mathbf{a}}{\|\mathbf{a}\|}; \quad K_n = \frac{1}{\|\mathbf{F} \cdot \mathbf{A}\|^2} (\mathbf{F} \cdot \mathbf{A} \cdot \mathbf{F} \cdot \boldsymbol{\kappa} \cdot \mathbf{F}^T \cdot \mathbf{F} \cdot \mathbf{A}) \quad (6)$$

It can be shown that through this operation, the bond vector depends on the in-plane strains and the bending strains. The shear strains are included through the director. The basic idea is that the director  $\mathbf{d}$  can be represented as a projection onto the normal vector  $\mathbf{n}$  and the base vectors  $\mathbf{g}_\alpha$ . If the formulas are re-arranged, one can identify the shear strains in the normal vector. This makes the normal vector dependent on the shear and in-plane strains, which makes the bond vector depended on all three REISSNER–MINDLIN strains.

$$s_{\mathbf{g}_\alpha} = \frac{1}{\|\mathbf{g}_\alpha\|} \mathbf{g}_\alpha \cdot \mathbf{d} = \frac{1}{\|\mathbf{g}_\alpha\|} \overline{\gamma_\alpha}; \quad s_{\mathbf{n}}^2 = 1 - (s_{\mathbf{g}_1} \|\mathbf{g}_1\|^2 + s_{\mathbf{g}_2} \|\mathbf{g}_2\|^2 + 2 s_{\mathbf{g}_1} s_{\mathbf{g}_2} \mathbf{g}_1 \cdot \mathbf{g}_2) \quad (7)$$

$$\mathbf{d} = s_{\mathbf{n}} \mathbf{n} + s_{\mathbf{g}_\alpha} \mathbf{g}_\alpha \rightarrow \mathbf{n} = \frac{1}{s_{\mathbf{n}}} (\mathbf{d} - s_{\mathbf{g}_\alpha} \mathbf{g}_\alpha) \quad (8)$$

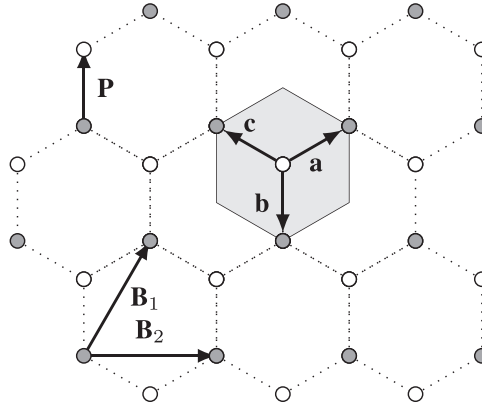


FIGURE 10 Lattice structure of graphene and representative cell.

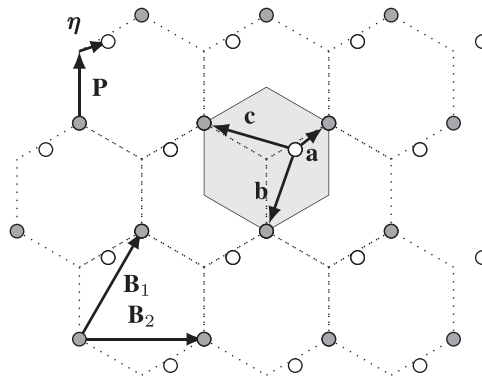


FIGURE 11 Inner displacement of graphene.

### 3.2 | Homogenisation procedure

A homogenisation procedure is used to derive the constitutive equation from the interatomic potentials. For this, a discrete representative cell of three bond vectors  $\mathbf{a}$ ,  $\mathbf{b}$ ,  $\mathbf{c}$  is considered (Figure 10). The strain energy density  $W$  of this cell is defined as the atomic site energy  $E_{\text{Atom}}$  divided by the surface of the cell  $S_0$ . As we only consider flat reference configurations, the area of the representative cell can be calculated with the standard cross product of the bond vectors. Due to the use of interatomic potentials, the result of this homogenisation procedure is a hyperelastic material model.

$$W = \frac{1}{S_0} E_{\text{Atom}}(\mathbf{a}, \mathbf{b}, \mathbf{c}); \quad S_0 = \|\mathbf{a} \times \mathbf{b}\| + \|\mathbf{a} \times \mathbf{c}\| + \|\mathbf{b} \times \mathbf{c}\| \quad (9)$$

### 3.3 | Internal relaxation

Graphene is a BRAVAIS multilattice [15]. It consists of two BRAVAIS single lattices shifted by the vector  $\mathbf{P}$  (Figure 10). Each single lattice is centrosymmetric. However, graphene is not centrosymmetric. The problem is that the CAUCHY–BORN rule is only valid for centrosymmetric crystals. So if we apply a homogeneous deformation to the reference cell, the displacement in the cell may not be homogeneous [16]. This results in the energy of the cell not being a local minimum. To correct this, we can move the reference atom until a local energy minimum is found (Figure 11). This process is called ‘internal relaxation’. We describe the motion with the internal degree of freedom  $\boldsymbol{\eta}$ . The shift at which the energy becomes minimal is  $\hat{\boldsymbol{\eta}}$ . The energy evaluated at the shift  $\hat{\boldsymbol{\eta}}$  is called relaxed strain-energy density  $\hat{W}$ . The internal relaxation is, therefore, a numerical minimisation problem (see Equation 10). We can solve this using the NEWTON–RAPHSON method with the update scheme given in Equation (11). Internal relaxation takes place in the tangent space of the reference configuration. This ensures the frame indifference. The shift  $\boldsymbol{\eta}$  describes the shift between the two BRAVAIS grids. Therefore, only the ref-

erence atom (the one in the centre) needs to be moved, as the other atoms are on the same single lattice. As a result, there are only two degrees of freedom (horizontal and vertical displacement). This makes the resulting system of equations easy to solve.

$$\hat{\boldsymbol{\eta}}(\boldsymbol{\varepsilon}, \boldsymbol{\kappa}, \boldsymbol{\gamma}) = \arg(\min_{\boldsymbol{\eta}} W(\boldsymbol{\varepsilon}, \boldsymbol{\kappa}, \boldsymbol{\gamma}, \boldsymbol{\eta})) \rightarrow \left. \frac{\partial W}{\partial \boldsymbol{\eta}} \right|_{\boldsymbol{\eta}=\hat{\boldsymbol{\eta}}} = \mathbf{0} \quad (10)$$

$$\Delta \boldsymbol{\eta} = - \left[ \frac{\partial^2 W}{\partial \boldsymbol{\eta} \partial \boldsymbol{\eta}} \right]^{-1} \frac{\partial W}{\partial \boldsymbol{\eta}} \quad (11)$$

### 3.4 | Stress resultant vector and tangential material matrix

The stress tensor and the tangential material tensor are calculated by deriving the relaxed strain-energy density. The derivation of the internal displacement vanishes due to the internal relaxation (10). To calculate the derivative of the relaxed strain-energy density, we simply calculate the derivative of the strain-energy density function and evaluate it at the internal displacement  $\hat{\boldsymbol{\eta}}$ . When considering, for example, the BRENNER potential (12), we need the derivatives of the strain-energy density with respect to the atomistic kinematics (bond length  $\|\mathbf{a}_i\|$ , valence angle  $\theta$ ) and the derivative of the atomistic kinematics with respect to the REISSNER–MINDLIN strains.

$$\frac{\partial \hat{W}}{\partial \boldsymbol{\varepsilon}} = \left( \frac{\partial W}{\partial \boldsymbol{\varepsilon}} + \frac{\partial W}{\partial \boldsymbol{\eta}} \frac{\partial \boldsymbol{\eta}}{\partial \boldsymbol{\varepsilon}} \right) \bigg|_{\boldsymbol{\eta}=\hat{\boldsymbol{\eta}}} = \frac{\partial W}{\partial \boldsymbol{\varepsilon}} \bigg|_{\boldsymbol{\eta}=\hat{\boldsymbol{\eta}}}; \quad \frac{\partial W}{\partial \boldsymbol{\varepsilon}} = \sum_{i=1}^3 \left[ \frac{\partial W}{\partial \|\mathbf{a}_i\|} \frac{\partial \|\mathbf{a}_i\|}{\partial \boldsymbol{\varepsilon}} + \frac{\partial W}{\partial \theta_i} \frac{\partial \theta_i}{\partial \boldsymbol{\varepsilon}} \right] \quad (12)$$

The stress resultant vector and the tangential material matrix result from the first and second derivatives. The first derivative with respect to the membrane, bending and shear strains gives the membrane, bending and shear stress resultants. The second derivative gives the corresponding entries in the tangential material matrix. Note that the non-diagonal entries must be zero as the stresses and strains must be decoupled (e.g., the membrane strains should not induce bending stresses).

$$\begin{bmatrix} \mathbf{n} \\ \mathbf{m} \\ \mathbf{q} \end{bmatrix} = \begin{bmatrix} \frac{\partial \hat{W}}{\partial \boldsymbol{\varepsilon}} \\ \frac{\partial \hat{W}}{\partial \boldsymbol{\kappa}} \\ \frac{\partial \hat{W}}{\partial \boldsymbol{\gamma}} \end{bmatrix} \quad \mathbb{C}_T = \begin{bmatrix} \frac{\partial^2 \hat{W}}{\partial \boldsymbol{\varepsilon} \partial \boldsymbol{\varepsilon}} & \frac{\partial^2 \hat{W}}{\partial \boldsymbol{\varepsilon} \partial \boldsymbol{\kappa}} & \frac{\partial^2 \hat{W}}{\partial \boldsymbol{\varepsilon} \partial \boldsymbol{\gamma}} \\ \frac{\partial^2 \hat{W}}{\partial \boldsymbol{\kappa} \partial \boldsymbol{\varepsilon}} & \frac{\partial^2 \hat{W}}{\partial \boldsymbol{\kappa} \partial \boldsymbol{\kappa}} & \frac{\partial^2 \hat{W}}{\partial \boldsymbol{\kappa} \partial \boldsymbol{\gamma}} \\ \frac{\partial^2 \hat{W}}{\partial \boldsymbol{\gamma} \partial \boldsymbol{\varepsilon}} & \frac{\partial^2 \hat{W}}{\partial \boldsymbol{\gamma} \partial \boldsymbol{\kappa}} & \frac{\partial^2 \hat{W}}{\partial \boldsymbol{\gamma} \partial \boldsymbol{\gamma}} \end{bmatrix} = \begin{bmatrix} \mathbb{C}_n & 0 & 0 \\ 0 & \mathbb{C}_m & 0 \\ 0 & 0 & \mathbb{C}_q \end{bmatrix} \quad (13)$$

The stress resultants and the tangent material matrix are passed back to the shell element after the calculation. An important point is that the units of the tensors must be equivalent to the units of the shell. The interatomic potentials have the unit Joule or force times length. The strain energy density is the energy of the interatomic potentials averaged for the representative cell, so the unit is force per length. The strains have different units. The membrane and shear strains have the unit 1. The bending strains have the unit 1 per length. The resulting units can be seen in Equation (14). They correspond to the stress resultant units of the continuum shell.

$$\begin{bmatrix} \mathbf{n} \\ \mathbf{m} \\ \mathbf{q} \end{bmatrix}_{\text{atomistic}} \leftarrow \begin{matrix} \text{[force/length]} \\ \text{[force} \cdot \text{length/length]} \\ \text{[force/length]} \end{matrix}; \quad \begin{bmatrix} \mathbf{n} \\ \mathbf{m} \\ \mathbf{q} \end{bmatrix}_{\text{shell}} \leftarrow \begin{matrix} \text{[force/length]} \\ \text{[force} \cdot \text{length/length]} \\ \text{[force/length]} \end{matrix} \quad (14)$$

## 4 | CONCLUSION

A hierarchical multi-scale approach to incorporate the information of a two-dimensional atomic lattice into a continuum shell model is presented. The extensions of the CAUCHY–BORN rule are also discussed. It is shown that existing approaches lead to KIRCHHOFF–LOVE shell models. The new approach presented allows REISSNER–MINDLIN shell models to be used with a standard ‘user material’ interface of existing FE-codes.



## ACKNOWLEDGMENTS

Open access funding enabled and organized by Projekt DEAL.

## ORCID

Julian Ochs  <https://orcid.org/0009-0009-4871-3951>

## REFERENCES

1. Pereira, V. M., Neto, A. C., Liang, H., & Mahadevan, L. (2010) Geometry, mechanics, and electronics of singular structures and wrinkles in graphene. *Physical Review Letters*, *105*(15), 156603.
2. Jain, N., Bansal, T., Durcan, C. A., Xu, Y., & Yu, B. (2013). Monolayer graphene/hexagonal boron nitride heterostructure. *Carbon*, *54*, 396–402.
3. Ponomarenko, L. A., Schedin, F., Katsnelson, M. I., Yang, R., Hill, E., Novoselov, K., & Geim, A. (2008). Chaotic Dirac billiard in graphene quantum dots. *Science*, *320*(5874), 356–358.
4. Miao, X., Tongay, S., Petterson, M., Berke, K., Rinzler, A. G., Appleton, B. R., & Hebard, A. F. (2012). High efficiency graphene solar cells by chemical doping. *Nano Letters*, *12*(6), 2745–2750.
5. Tildesley, D. J., & Allen, M. P. (1987). *Computer simulation of liquids*. Clarendon.
6. Wackerfuß, J. (2009). Molecular mechanics in the context of the finite element method. *International Journal for Numerical Methods in Engineering*, *77*(7), 969–997.
7. Wackerfuß, J., & Niederhöfer, F. (2019). Using finite element codes as a numerical platform to run molecular dynamics simulations. *Computational Mechanics*, *63*(2), 271–300.
8. Cousins, C. (1978). Inner elasticity. *Journal of Physics C: Solid State Physics*, *11*(24), 4867.
9. Ericksen, J. (1984). *Phase transformations and material instabilities in solids*. Elsevier Science.
10. Guo, X., Wang, J., & Zhang, H. (2006). Mechanical properties of single-walled carbon nanotubes based on higher order Cauchy–Born rule. *International Journal of Solids and Structures*, *43*(5), 1276–1290.
11. Arroyo, M., & Belytschko, T. (2002). An atomistic-based finite deformation membrane for single layer crystalline films. *Journal of the Mechanics and Physics of Solids*, *50*(9), 1941–1977.
12. Findeisen, C., & Wackerfuß, J. (2016). A general approximation of the exponential Cauchy–Born hypothesis to model arbitrarily shaped shell-like nanostructures within continuum mechanics. *International Journal for Numerical Methods in Engineering*, *105*(10), 747–780.
13. Hollerer, S., & Celigoj, C. C. (2013). Buckling analysis of carbon nanotubes by a mixed atomistic and continuum model. *Computational Mechanics*, *51*, 765–789.
14. Cirak, F., Ortiz, M., & Schröder, P. (2000). Subdivision surfaces: A new paradigm for thin-shell finite-element analysis. *International Journal for Numerical Methods in Engineering*, *47*(12), 2039–2072.
15. Arroyo, M., & Belytschko, T. (2004). Finite crystal elasticity of carbon nanotubes based on the exponential Cauchy–Born rule. *Physical Review B*, *69*(11), 115415.
16. Peng, Z., Yonggang, H., Geubelle, P. H., & Kehchih, H. (2002). On the continuum modeling of carbon nanotubes. *Acta Mechanica Sinica*, *18*, 528–536.

**How to cite this article:** Ochs, J., & Wackerfuß, J. (2023). Continuous modelling of single layer 2D carbon nanostructures based on a modified Cauchy–Born rule. *Proceedings in Applied Mathematics and Mechanics*, *23*, e202300197. <https://doi.org/10.1002/pamm.202300197>